Science
AAAS

Clonogenic Neoblasts Are Pluripotent Adult Stem Cells That Underlie Planarian Regeneration

Daniel E. Wagner, *et al.*

Science **332**, 811 (2011);
DOI: 10.1126/science.1203983

Science (print ISSN 0036-8075; online ISSN 1095-9203) is published weekly, except the last week in December, by the American Association for the Advancement of Science, 1200 New York Avenue NW, Washington, DC 20005.

Clonogenic Neoblasts Are Pluripotent Adult Stem Cells That Underlie Planarian Regeneration

Daniel E. Wagner,[1]* Irving E. Wang,[1]* Peter W. Reddien[1]†

Pluripotent cells in the embryo can generate all cell types, but lineage-restricted cells are generally thought to replenish adult tissues. Planarians are flatworms and regenerate from tiny body fragments, a process requiring a population of proliferating cells (neoblasts). Whether regeneration is accomplished by pluripotent cells or by the collective activity of multiple lineage-restricted cell types is unknown. We used ionizing radiation and single-cell transplantation to identify neoblasts that can form large descendant-cell colonies in vivo. These clonogenic neoblasts (cNeoblasts) produce cells that differentiate into neuronal, intestinal, and other known postmitotic cell types and are distributed throughout the body. Single transplanted cNeoblasts restored regeneration in lethally irradiated hosts. We conclude that broadly distributed, adult pluripotent stem cells underlie the remarkable regenerative abilities of planarians.

Pluripotent cells, such as embryonic blastomeres, differentiate into mature cell types spanning three germ layers (*1*–*3*). Although essential for development, pluripotent cells are generally not known to be present in adult animals (*4*, *5*). Adult tissues, in contrast, are typically maintained by specialized, tissue-specific adult stem cells (*5*–*11*). Planarians are flatworms well known for the ability to regenerate whole animals from small pieces of tissue (*12*). Planarian regeneration requires a population of proliferative cells, historically known as neoblasts, that exist throughout the body and collectively produce all known differentiated cell types (*13*, *14*). Neoblasts have great potential for molecular genetic studies in *Schmidtea mediterranea*, in which a sequenced genome and molecular tools (including RNA interference technology) enable the identification and study of genes controlling regeneration (*14*, *15*). To date, however, neoblast properties have only been studied at the level of a population (*14*, *16*–*21*). The cell population known as neoblasts, therefore, could either contain only lineage-restricted cells that together allow regeneration or could contain, within the population, stem cells that are pluripotent at the single-cell level. A fundamental issue to address for understanding planarian regeneration, therefore, is the in vivo potential of individual proliferating planarian cells.

Colonies are generated from single *smedwi-1*$^+$ cells after irradiation. With the use of ionizing radiation, we developed an in vivo method that permits the study of rare, individual proliferating cells and their descendants (*22*). Irradiation eliminates dividing cells and is a classic strategy for studying stem cells (*23*, *24*). All dividing cells in adult planarians express the *smedwi-1* gene (Fig. 1A) (*25*); these cells are specifically, rapidly, and completely depleted after exposure to high irradiation doses (for example, 6000 rad) (*17*, *25*, *26*). Low irradiation doses (such as 500 rad) eliminate some proliferating cells, leaving a large number spread ventrally throughout the animal (*19*). We identified an irradiation dose (1750 rad) that eliminated all *smedwi-1*$^+$ cells from most (78%) animals (Fig. 1B). However, 7 days after 1750-rad exposure, rare *smedwi-1*$^+$ cells were present in the minority of animals (22%) as sparse "clusters" (Fig. 1, B and C). Clusters consistently displayed compact, isolated, colonylike morphology and originated ventrally throughout the body (Fig. 1D and fig. S1, A to C) but were not associated with specific known tissues (fig. S1, D and E). If resulting from clonal growth of single *smedwi-1*$^+$ cells, these clusters provide the opportunity to study the developmental potential of individual planarian cells.

Numerous *smedwi-1*$^+$ cluster attributes indicate they result from clonal growth. *smedwi-1*$^+$ clusters were preceded by isolated *smedwi-1*$^+$ cells present 3 to 4 days after irradiation and typically displayed 3 to 10 cells after one week (Fig. 1, E and F). Based on the low proportion of animals with *smedwi-1*$^+$ cells in close proximity 3 days post-irradiation with 1750 rad (fig. S2), it is improbable that clusters arose from multiple adjacent *smedwi-1*$^+$ cells ($P = 0.0138$, two-tailed Fisher's exact test). Cluster size increased dramatically over time, suggesting exponential growth and ultimately yielding hundreds of *smedwi-1*$^+$ cells 14 to 18 days post-irradiation (Fig. 1, E and F). Consistent with clusters originating from preexisting *smedwi-1*$^+$ cells that survived irradiation, a cluster-location scatter plot resembled the normal *smedwi-1*$^+$ expression pattern (Fig. 1D), and cluster frequency decreased with increasing irradiation doses (see below). Bromodeoxyuridine (BrdU) delivery labels *smedwi-1*–expressing cells (fig. S3A) (*25*), followed by a rapid decline in incorporation within 24 to 48 hours (fig. S3, B to D) (*17*), demonstrating that unincorporated BrdU does not persist over the long term. A BrdU pulse followed by irradiation resulted in clusters consisting entirely of BrdU$^+$; *smedwi-1*$^+$ cells (fig. S3E), indicating that *smedwi-1*$^+$ cluster expansion results from division of existing *smedwi-1*$^+$ cells (i.e., by clonal growth). If some other process, such as dedifferentiation, had produced *smedwi-1*$^+$ cluster cells, these cells should have been BrdU$^-$.

After irradiation, every proliferative cell detected by an 8-hour BrdU pulse (Fig. 1G)—or by using probes for the conserved proliferation marker genes *histone h2b* (*Smed-h2b*) (*27*), *pcna* (*Smed-pcna*) (*28*), or *ribonucleotide reductase* (*Smed-RRM2-1*) (fig. S3, F to H) (*17*, *29*)—existed in clusters and expressed *smedwi-1* (n = 815/815 cells). Therefore, no other source (non-*smedwi-1*$^+$) for proliferating cells exists outside of *smedwi-1*$^+$ clusters in irradiated animals. Furthermore, if additional sources for *smedwi-1*$^+$ cells (other than clonal growth) existed, the cluster number would be expected to increase with time and small, newly formed clusters might be present at late time points after irradiation. Neither of these possibilities was observed (Fig. 1F). New cluster production was also not observed after amputation or feeding (fig. S4), which elicit proliferative responses (*30*, *31*). These data indicate that clonal expansion (producing colonies) represents the source of new *smedwi-1*$^+$ dividing cells during cluster formation and growth.

Not all proliferating cells (neoblasts) necessarily have the capacity to form colonies. We term cells displaying this capacity "clonogenic neoblasts" (cNeoblasts); these cells express *smedwi-1*, have a body-wide (head-to-tail) distribution (Fig. 1D), and generate large, expanding colonies of *smedwi-1*$^+$ cells. The ability of small numbers of colonies to ultimately restore both *smedwi-1*$^+$ cells and mitotic activity to normal levels (fig. S5) suggests a stem cell–like capacity for self-renewal.

To investigate the potential of individual cNeoblasts, we used three well-established differentiation assays involving a SMEDWI-1 antibody (*25*, *30*, *32*), BrdU pulse-chase (*17*, *18*, *32*), and postmitotic cell type markers (*17*, *30*, *32*, *33*) to analyze *smedwi-1*$^+$ colonies. SMEDWI-1 protein is present in *smedwi-1* mRNA$^+$ dividing cells and temporarily remains detectable in postmitotic descendant cells (*25*). Therefore, differentiating cells transit through a SMEDWI-1(protein)$^+$; *smedwi-1*(mRNA)$^-$ state (*30*, *32*). All colonies examined (n = 12/12 colonies) contained SMEDWI-1$^+$; *smedwi-1*$^-$ cells (Fig. 1H). Independently, BrdU can label cells that divide and exit the *smedwi-1*$^+$ state. All colonies analyzed by 4-day BrdU pulse-chase (n = 31/31 colonies) contained BrdU$^+$;

[1]Howard Hughes Medical Institute, Department of Biology, Massachusetts Institute of Technology (MIT), Whitehead Institute for Biomedical Research, 9 Cambridge Center, Cambridge, MA 02142, USA.

*These authors contributed equally to this work.
†To whom correspondence should be addressed. E-mail: reddien@wi.mit.edu

smedwi-1^{-} cells (Fig. 2), and no BrdU^{+} cells existed in worms lacking *smedwi-1*$^{+}$ colonies (n = 25/25 animals), indicating that colonies produce and are the only source for cells exiting the *smedwi-1*$^{+}$ undifferentiated state. SMEDWI-1^{+} or BrdU^{+} colony cells can thus be assessed for lineage-specific marker expression to determine the developmental potential of individual cNeoblasts.

cNeoblasts display broad differentiation capacity. Described adult stem cells typically produce only differentiated cells corresponding to their germ layer and tissue of origin (*5*). To address whether cNeoblasts, in contrast, could produce cell types derived from multiple germ layers, we identified and characterized markers for neuronal (ectoderm-derived) and intestinal (endoderm-derived) lineages. In untreated animals, some SMEDWI-1^{+} descendant cells expressed a choline acetyl-transferase ortholog, *Smed-chat* (fig. S6); *chat* expression is widely conserved in cholinergic neurons (*34*). SMEDWI-1^{+}; *chat*$^{+}$ cells were enriched in brain regions and had neuronal morphology, and *chat*$^{+}$ cells coexpressed additional neuronal markers (fig. S6), indicating that SMEDWI-1^{+}; *chat*$^{+}$ cells are differentiating neurons. *Smed-gata4/5/6* and *Smed-hnf4*, orthologs of endoderm-promoting GATA4/5/6 and HNF4 transcription factors, respectively (*35*), were expressed in intestinal cells and also in interspersed cells surrounding the intestine (figs. S7 to S10). Many of these interspersed cells were irradiation-sensitive and SMEDWI-1^{+}, indicating that they represent differentiating endodermal cells (figs. S8 and S10). A third endoderm marker gene, *Smed-mat*, was expressed in intestinal branches (figs. S8 and S10). Finally, additional differentiation marker genes (*Smed-AGAT-1*, NB.21.11E, *Smed-MCP-1*, *Smed-ODC-1*, *Smed-CYP1A1-1*, and NB.52.12F) are expressed in partially overlapping mesenchymal populations of postmitotic cells (fig. S11, A to F) (*17*). These populations have unknown lineage relationships but turn over rapidly and are consequently depleted after irradiation (fig. S11, G to L) (*17*).

Using the SMEDWI-1 antibody to label colony cell descendants, we examined individual colonies for the presence of both *gata4/5/6*$^{+}$ and *chat*$^{+}$, both *gata4/5/6*$^{+}$ and *AGAT-1*$^{+}$, or both *AGAT-1*$^{+}$ and *chat*$^{+}$ differentiating cells. In nearly all cases (n = 20/22 colonies), individual colonies contained newly produced cells of both lineages that we tested (Fig. 2, A to C and fig. S12). The 1750-rad dose yields rare, well-separated colonies (Fig. 1C); animals fixed 7 days after irradiation contained single colonies (n = 12/28 animals), no colonies (n = 12/28 animals), and, only rarely, more than one colony (n = 4/28 animals). Given the high frequency of colonies producing multiple lineages (n = 20/22 colonies), it is improbable that all such cases were the result of multiple colonies merging ($P < 0.0001$, Fisher's exact test). In addition, we used a 4-day BrdU pulse chase as an independent method to identify several colonies containing both BrdU^{+}; *chat*$^{+}$ (neuronal) and BrdU^{+}; *mat*$^{+}$ (intestinal) cells (Fig. 2D). Nearly all colonies examined, using the SMEDWI-1 antibody or BrdU, produced differentiated cells for any single lineage analyzed (n = 61/64 colonies) (fig. S13). These colonies were distributed throughout the body and not restricted to specific anatomical regions (Fig. 2E). Finally, nearly every *smedwi-1*$^{+}$ colony examined had associated cells expressing every additional differentiation marker that we tested (NB.21.11E, *MCP-1*, *ODC-1*, *CYP1A1-1*, NB.52.12F, *AGAT-1*) (n = 110/115 colonies) (fig. S14, A to F). Furthermore, descendant cell clusters were never observed in regions lacking *smedwi-1*$^{+}$ colonies (fig. S11, G to L). In addition, even early colonies (7 days post-irradiation) had associated differentiated cells (fig. S14G). Together, these data indicate that broad multipotency and a body-wide distribution are fundamental attributes of individual cNeoblasts.

Small numbers of cNeoblasts restore regenerative ability. Irradiated planarians cannot regenerate (*36*) and suffer massive tissue loss because of failed replacement of aged differentiated cells (*36*, *37*). However, transplantation of large numbers of cells (*16*) or tissue fragments can restore regenerative ability to irradiated hosts and change sexual behavior to that of the donor (*16*, *20*, *21*, *38*). We sought to determine whether small numbers of cNeoblasts would restore regenerative ability to irradiated animals. After irradiation, some animals were fixed and colony

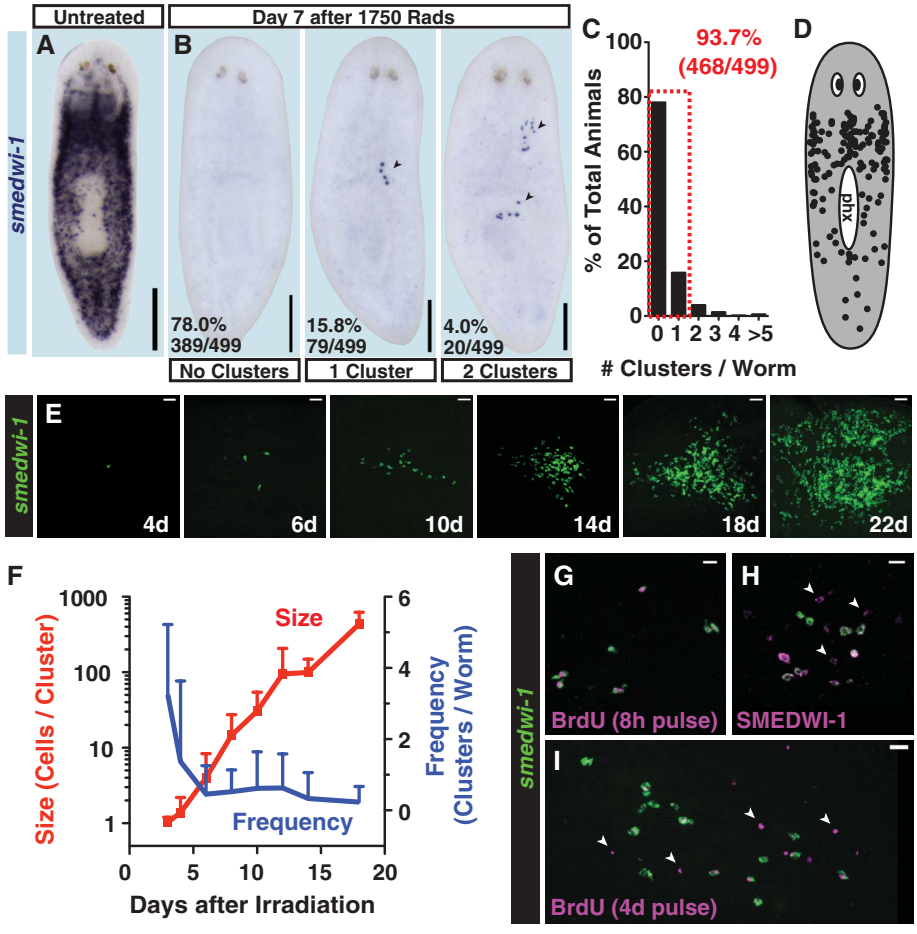

Fig. 1. Expanding colonies are generated from isolated *smedwi-1*$^{+}$ cells after irradiation. (**A** and **B**) Proliferating cells were detected by *smedwi-1* expression using whole-mount in situ hybridization (ISH). Anterior, up; ventral surface shown. (B) Representative images 7 days after 1750-rad treatment show clusters (arrowheads) of *smedwi-1*$^{+}$ cells (individual purple dots). (**C**) Histogram of cluster frequencies after 1750-rad treatment. The dashed red box indicates that the majority of animals contained either zero or one cluster. (**D**) Clusters observed by *smedwi-1* ISH 7 days post–1750-rad treatment displayed in a scatter plot. phx, pharynx. (**E** and **F**) Animals fixed in a time course after 1750-rad treatment analyzed by *smedwi-1* fluorescence in situ hybridization (FISH). d, days. (F) Mean cluster frequency (number of clusters per worm) and size (number of *smedwi-1*$^{+}$ cells per cluster) are plotted. Error bars indicate SD (n = 17 to 22 animals per time point). (**G**) Immunofluorescence (IF) (BrdU) and FISH (*smedwi-1*). 234/234 BrdU^{+} cells (8-hour BrdU pulse in 7-day–irradiated worms) were *smedwi-1* positive. (**H**) IF (SMEDWI-1) and FISH (*smedwi-1*); 12/12 colonies contained SMEDWI-1^{+}; *smedwi-1*$^{-}$ cells (arrowheads) 7 days post–1750-rad treatment. (**I**) IF (BrdU) and FISH (*smedwi-1*). 31/31 colonies (with BrdU pulse days 7 to 11 post-1750 rad) contained BrdU^{+}; *smedwi-1*$^{-}$ cells. Scale bars, 200 μm [(A) and (B)]; 20 μm [(E) and (G) to (I)].

numbers determined; the remaining animals were followed to assess survival and regeneration frequencies. Increasing irradiation doses resulted in decreasing colony numbers (Fig. 3, A and B) and survival rates (fig. S15A). Regeneration, which involves the production of diverse cell types (fig. S16), was initially impeded in animals cut 4 days post-irradiation (fig. S15, B and C); however, many animals both survived and ultimately regenerated at doses that produced sparse, measurable colony numbers (Fig. 3, A to D and table S1). These animals regenerated heads containing neurons (ectoderm), muscle (mesoderm), and intestine (endoderm) (Fig. 3, D and E). The minimum number of cNeoblasts initially present in irradiation survivors can be estimated by comparing the number of colonies present (in fixed animals) to observed regeneration frequencies (see table S1). Our data indicate as few as three ($P = 0.0478$), four ($P = 0.0017$), or five colonies ($P < 0.0001$, Fisher's exact test) can be sufficient to restore regenerative ability to entire animals.

Transplantation of individual cNeoblasts. To determine whether a single cNeoblast can generate all essential adult cells, we developed a method for isolating and transplanting individual cNeoblasts into lethally irradiated hosts. Previous flow cytometry studies identified an irradiation-sensitive cell population (the X1 fraction) with a high percentage of *smedwi-1*$^+$ cells (*26*, *39*). However, the Hoechst 33342 DNA dye used in this method is cytotoxic. Therefore, size and complexity properties of cells within the X1 fraction were used to define a gate for sorting unlabeled cells, which we refer to as the X1(FS) fraction (Fig. 4, A and B).

X1(FS) cells are heterogeneous; however, cells with a similar morphology to X1 cells can be identified microscopically (Fig. 4C). Single selected cells were loaded into needles and transplanted postpharyngeally into lethally irradiated hosts (Fig. 4D). To confirm that only single cells were transplanted, needles were loaded and the contents expelled into media. In all cases, only a single cell was observed exiting the needle (n = 136/136 test ejections). Furthermore, some animals were fixed immediately after transplant and labeled with a *smedwi-1* RNA probe. All injected animals had either one (n = 20/60 animals) or zero (n = 40/60 animals) *smedwi-1*$^+$ cells (Fig. 4, E and F).

If a transplanted cell was a cNeoblast capable of engraftment, then clonal growth of progeny cells would be expected. Indeed, animals examined 6 days after single-cell transplantation displayed clusters with 1 to 13 *smedwi-1*$^+$ cells (n = 23/100 animals) (Fig. 4G). Furthermore, selecting for X1(FS) cells that were approximately 10 μm in diameter and had blebs and/or cytoplasmic processes increased engraftment rates, which ranged from 12% (n = 2/17 animals) to 75% (n = 15/20 animals) (fig. S17). Cells with properties of cNeoblasts, therefore, are present in the X1(FS) fraction and can be successfully transplanted.

If cNeoblasts are pluripotent stem cells capable of self-renewal, then a single cNeoblast should, in principle, be capable of restoring tissue turnover and regenerative capacity to lethally irradiated hosts. However, for this to occur the irradiated host must survive long enough for the cNeoblast to repopulate the *smedwi-1*$^+$ population and replenish dying tissue. Therefore, we used a sexual *S. mediterranea* strain (S2F1L3F2) that can survive longer than the asexual strain (CIW4) after a 6000-rad irradiation dose (fig. S18). Sexual hosts transplanted with single asexual cells had colonies consisting of large numbers of SMEDWI-1$^+$ cells 30 days after transplantation (n = 4/17 animals) (Fig. 4H). Every colony examined contained SMEDWI-1$^+$; *Smed-gata4/5/6*$^+$ double-positive cells (n = 4/4 colonies), and most of these colonies also contained SMEDWI-1$^+$; *Smed-chat*$^+$ double-positive cells (n = 3/4 colonies) (Fig. 4H). Transplant data thus independently confirm attributes of colonies described post–1750 rad, further indicating that clonal growth and multipotency are important features of individual cNeoblasts.

Entire animals and strains regenerated from a single transplanted cNeoblast. Two weeks after irradiation, lesions appeared at sexual animal head tips, followed by progressive anterior-to-posterior tissue regression with 100% penetrant animal death after approximately 6 weeks (n = 78/78 animals) (Fig. 5A). Remarkably, several transplant recipients lived past 7 weeks and eventually developed blastemas at the site of tissue regression (n = 7/130 animals) (Fig. 5A). Animals that developed blastemas regenerated anterior and mid-body structures, such as photoreceptors and pharynges (Fig. 5A), and regained feeding behavior by 8 weeks after irradiation. Of the seven rescued animals, three were expanded into strains (R1, R2, and R3) by serial amputation

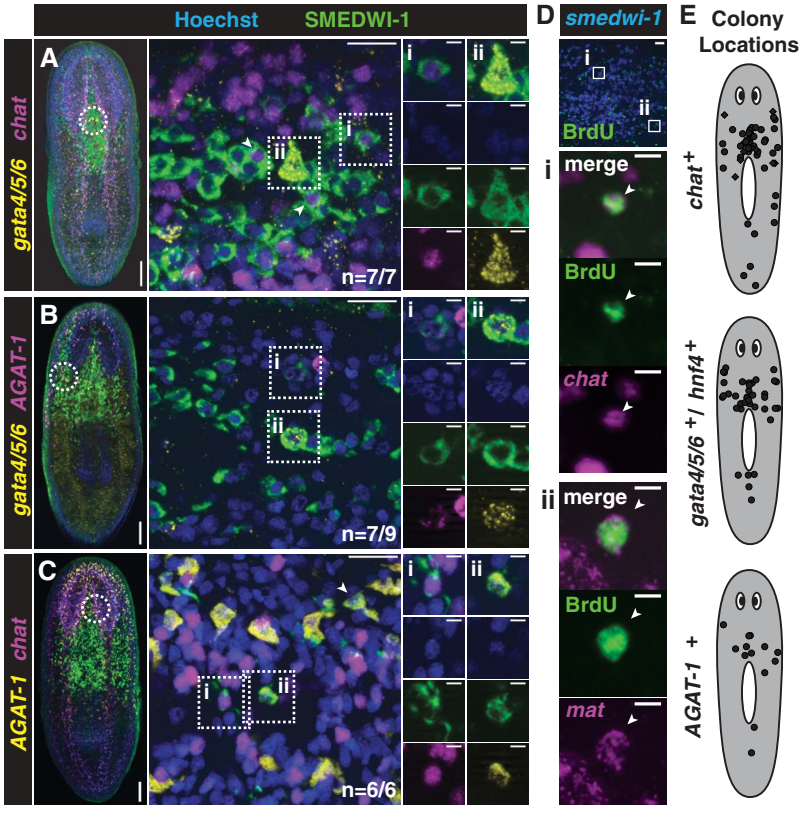

Fig. 2. Clonogenic neoblasts display broad differentiation capacity. (**A** to **C**) Triple-labeling of individual colonies 22 days after irradiation. Projections through optical sections from irradiated animals are shown here. (Left) Tiled images (images from overlapping regions assembled) of representative animals with individual colonies (anterior, up). Dotted circles indicate the approximate location of regions imaged at high magnification (middle panels); the middle images are optical sections with anterior to the right. Example differentiating cells from individual colonies labeled by IF (SMEDWI-1) and double FISH for *gata4/5/6* and *chat* (A), *gata4/5/6* and *AGAT-1* (B), or *AGAT-1* and *chat* (C) are shown. Proportions of colonies displaying multiple differentiating cell types are indicated. Roman numerals indicate double-positive cells, with individual channels shown in columns to the right. Additional double-positive cells are indicated by arrowheads (see also fig. S12). (**D**) IF (BrdU) and double FISH (*Smed-chat; Smed-mat*) worms with BrdU-pulse days 14 to 18 after irradiation. Single colonies (n = 7/7 colonies) contained both BrdU$^+$; *chat*$^+$ (neuronal) and BrdU$^+$; *mat*$^+$ (intestinal) descendants. Boxes indicate zoomed-in regions. (**E**) Scatter plots showing locations of individual colonies producing differentiated cell types (see also fig. S13). Colony cell differentiation was assessed by labeling with SMEDWI-1 (circles) or BrdU (diamonds). Scale bars, (A to C) left, 100 μm; middle 20 μm; right 5 μm; (D) top image, 20 μm; others, 5 μm.

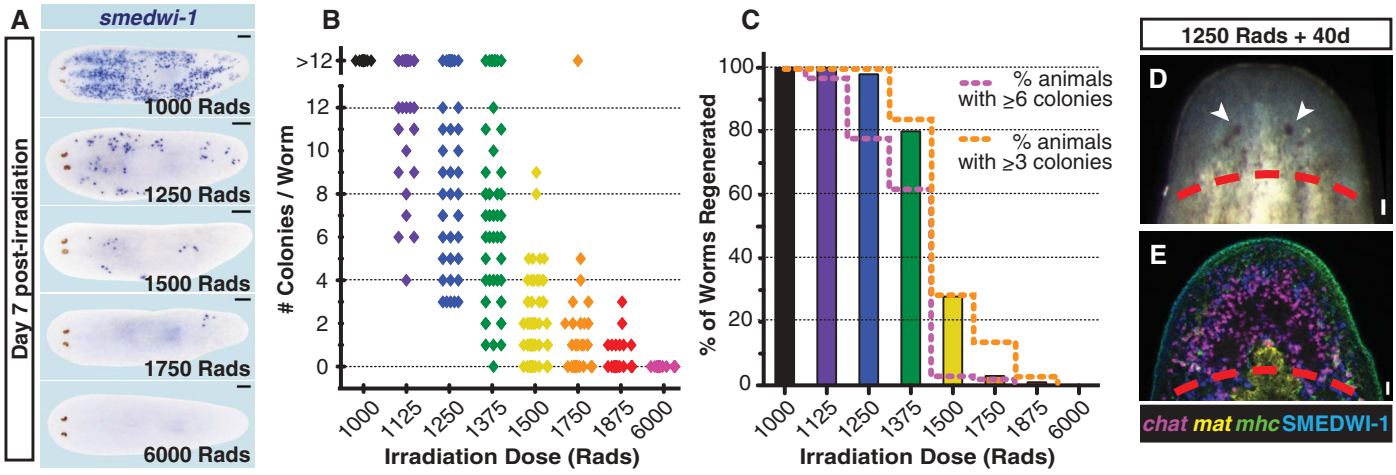

Fig. 3. Small numbers of cNeoblasts can restore tissue turnover and regenerative ability. (**A** and **B**) Animals were irradiated at different doses. Some of these animals were fixed 7 days post-irradiation (1000 rad, 25 animals; between 1125 and 1875 rad, >38 animals per dose; for 6000 rad, 26 animals) and labeled by *smedwi-1*$^+$ ISH. (A) Representative *smedwi-1*$^+$ ISH images. Anterior, left. (B) Colony numbers per worm are plotted (each dot represents one animal). (**C**) Percentage of animals with restored regeneration after irradiation is shown [≥98 worms per dose were examined; animals were from the same irradiated cohort as in (A) and (B)]. Data indicate that three or more cNeoblasts were sufficient to restore regeneration (see also table S1). (**D**) Normal head regeneration in 97/99 worms amputated 39 or 40 days after 1250-rad treatment. Arrowheads denote photoreceptors. (**E**) Heads regenerated after irradiation contained differentiated neuronal (*chat*$^+$), intestinal (*mat-1*$^+$), and muscle (*mhc-1*$^+$) cells (41/41 worms, 1250 rad; 15/15 worms, 1500 rad). SMEDWI-1$^+$ cells were also restored (n = 9/9 worms, 1250 rad). Dotted lines denote the approximate amputation plane. Scale bars, 200 μm (A); 20 μm [(D) to (E)].

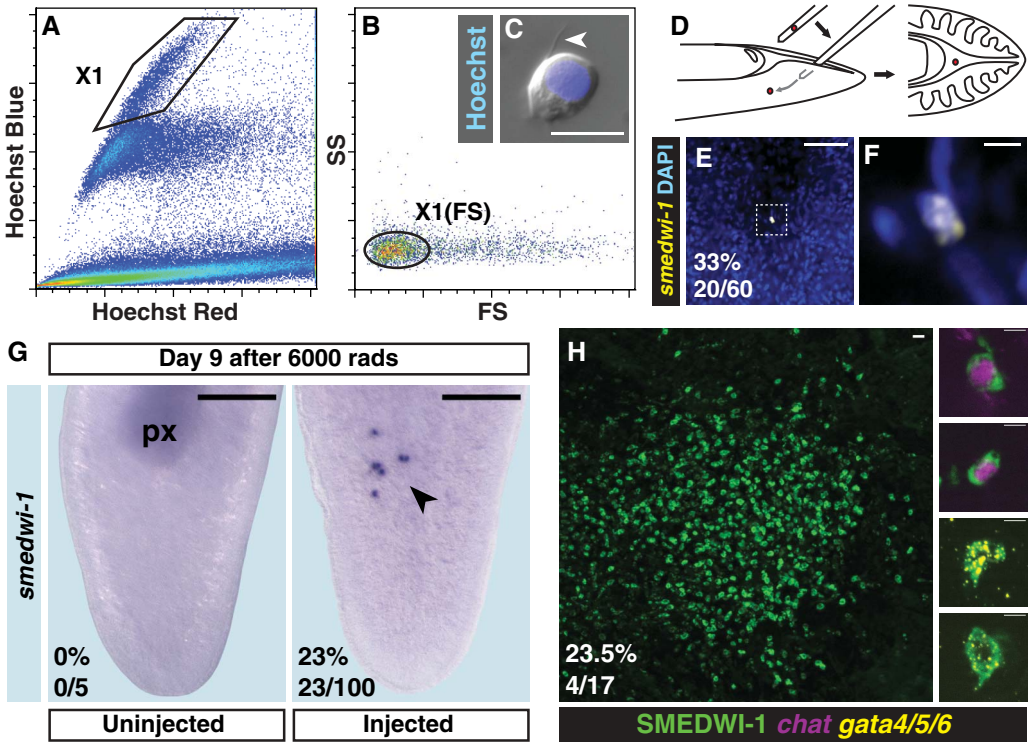

Fig. 4. Single transplanted cNeoblasts display properties of clonal growth and multipotency. Irradiation-sensitive cells (polygonal gate) were identified by Hoechst 33342 labeling (**A**) and back-gated to set the X1(FS) gate (oval) based on size (FS) and complexity (SS) parameters (**B**). The X1(FS) fraction is heterogeneous and contains some cells approximately 10 μm in diameter with processes (arrowhead) (**C**). (**D**) Individual cells were loaded into needles (one needle used per injection) and transplanted into the medial, postpharyngeal, parenchymal space of hosts. (**E** and **F**) FISH (*smedwi-1*) of a host immediately after transplantation. Anterior, up. The ventral surface is shown. Zero (n = 40/60 animals) or one (n = 20/60 animals) *smedwi-1*$^+$ cells were observed in all cases, with expected size and morphology. (F) is a zoomed-in image of (E). (**G**) Colony formation 9 days after irradiation, 6 days after transplant. Anterior, up. The ventral surface is shown. Colonies of *smedwi-1*$^+$ cells (arrowhead) appeared in transplant recipients (n = 23/100 animals) but not in untreated animals (n = 0/5 animals). px, pharynx. (**H**) IF (SMEDWI-1) and double FISH (*Smed-gata4/5/6*; *Smed-chat*) 33 days after irradiation, 30 days after transplant. Single colonies were observed (n = 4/17 animals); example differentiating cells from displayed colony are shown. Scale bars, 10 μm (C); 50 μm (E); 5 μm (F) and zoomed images in (H); 20 μm (H); 200 μm (G).

and regeneration (fig. S19). These animals exhibited normal blastema formation and the capacity to regenerate photoreceptors and intestine after amputation (Fig. 5B). The ability to produce multiple regenerating animals from a single transplanted cell indicates a self-renewing capability of cNeoblasts. Rescued strains did not display sexual features, such as large size and a gonopore; in contrast, animals in all three strains reproduced by binary fission, an asexual behavior seen very rarely in sexual animals (fig. S19).

To confirm that all new tissue in rescued strains resulted from clonal division from the donor cNeoblast, we genotyped the animals using single-nucleotide polymorphisms (SNPs) identified between the asexual strain and the sexual strain (*22*). Genomic DNA was isolated from strain R1, R2, and R3 animals after two rounds of regeneration; growth and regeneration should replace host tissues with donor-derived cells (Fig. 6A). If, on the other hand, host cells continue to replenish tissues

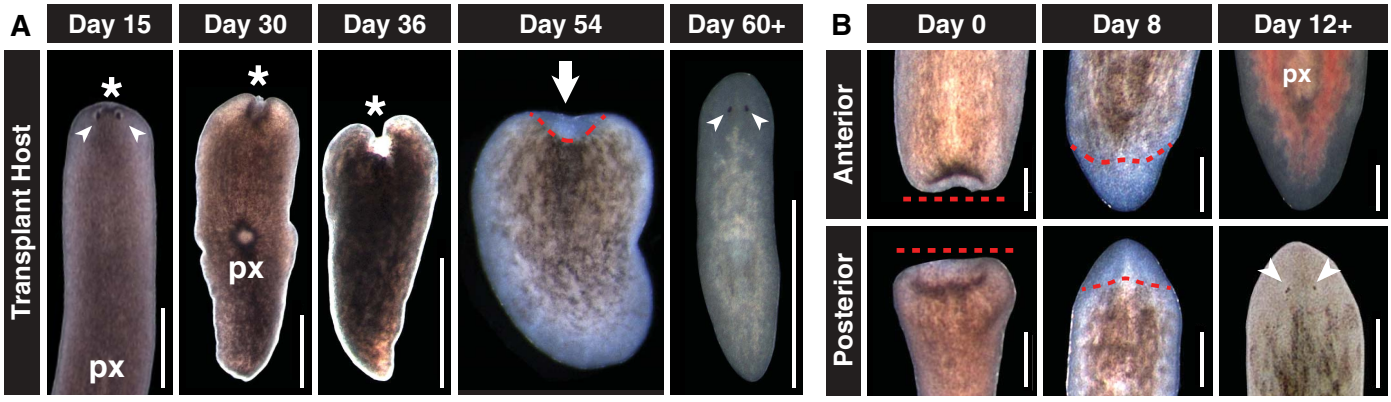

Fig. 5. Restoration of regeneration in lethally irradiated hosts by single transplanted cNeoblasts. (**A**) Representative images of transplant hosts. Tissue regression (asterisks) began anterior to photoreceptors (arrowheads) and progressed from anterior to posterior (px, pharynges). Rescued animals developed blastemas (arrow) at the regression site (red dotted line) after 7 weeks and fully regenerated after 8 weeks. Anterior, up. The dorsal surface is shown. (**B**) Representative images of rescue strains undergoing regeneration after amputation. Blastemas formed at approximate amputation plane (red dotted line). Intestine (labeled with red food coloring) and photoreceptors (arrowheads) were observed in blastemas after 12 days of regeneration. Anterior, up. The dorsal surface is shown. Scale bars, 1 mm (A); 500 μm (B).

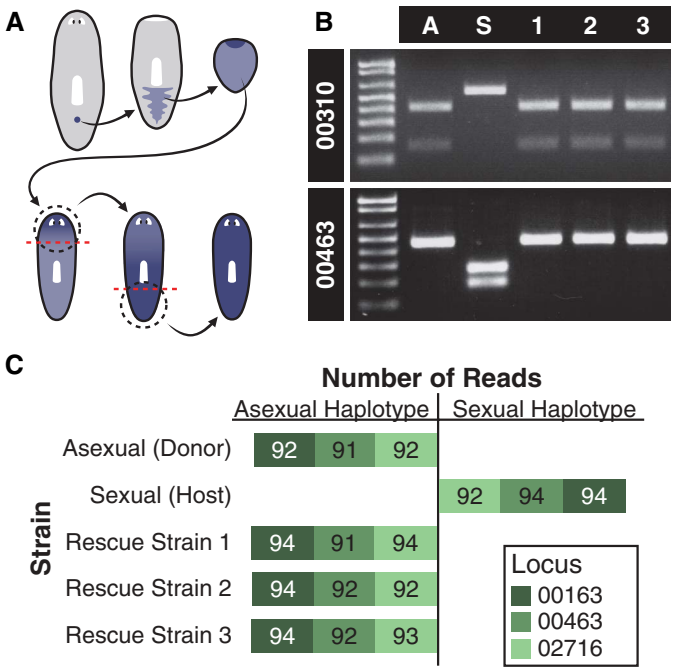

Fig. 6. Genotype conversion by single transplanted cNeoblasts. (**A**) Schematic showing replacement of host tissue by transplanted donor cells (blue); animals for genotyping were amputated (dotted lines) and allowed to regenerate twice. (**B**) PCR-RFLP analysis of rescued strains. Locus 00310 was cut by HpaI in asexual animals (A) and the rescued strains (1, 2, 3), but not in sexual animals (S). Locus 00463 was cut by ScaI in sexual animals, but not in asexual animals or the rescued strains. (**C**) Haplotype sequencing (*22*). Stacked histogram representing the number of sequencing reads from each locus for each strain. Bars extend left for number of reads corresponding to the asexual haplotype and right for number of reads corresponding to the sexual haplotype. Bar absence indicates no reads.

after irradiation, host SNPs in the collected genomic DNA would be expected. Polymerase chain reaction-restriction fragment length polymorphism (PCR-RFLP) analysis of two loci (RFLP 00310 and RFLP 00463) revealed that the rescued strains have the asexual strain RFLPs, indicating that the majority of cells in these animals were donor-derived (Fig. 6B). Sequencing of three independent homozygous haplotypes (00163, 00463, and 02716), each containing six SNPs that distinguish asexual CIW4 and sexual S2F1L3F2 strains, confirmed that the rescue strains possessed the donor rather than host genotype (Fig. 6C). These data indicate that descendants of a single cNeoblast ultimately transformed the recipient into a genetic clone of the donor by replacing all cells present in the original host. We conclude that cNeoblasts are pluripotent stem cells with a broad, body-wide distribution and that persistence into adulthood of pluripotent stem cells enables the extraordinary regenerative feats of planarians.

References and Notes

1. M. J. Evans, *J. Embryol. Exp. Morphol.* **28**, 163 (1972).
2. M. J. Evans, M. H. Kaufman, *Nature* **292**, 154 (1981).
3. G. R. Martin, *Proc. Natl. Acad. Sci. U.S.A.* **78**, 7634 (1981).
4. A. J. Wagers, R. I. Sherwood, J. L. Christensen, I. L. Weissman, *Science* **297**, 2256 (2002); 10.1126/science.1074807.
5. A. J. Wagers, I. L. Weissman, *Cell* **116**, 639 (2004).
6. I. L. Weissman, *Cell* **100**, 157 (2000).
7. G. J. Spangrude, S. Heimfeld, I. L. Weissman, *Science* **241**, 58 (1988).
8. N. Uchida *et al.*, *Proc. Natl. Acad. Sci. U.S.A.* **97**, 14720 (2000).
9. C. Blanpain, W. E. Lowry, A. Geoghegan, L. Polak, E. Fuchs, *Cell* **118**, 635 (2004).
10. B. Ohlstein, A. Spradling, *Nature* **439**, 470 (2006).
11. N. Barker *et al.*, *Nature* **449**, 1003 (2007).
12. T. H. Morgan, *Arch. Entw. Mech. Org.* **7**, 364 (1898).
13. J. Keller, *Jen Zeit Naturw* **28**, 370 (1894).
14. P. W. Reddien, A. Sánchez Alvarado, *Annu. Rev. Cell Dev. Biol.* **20**, 725 (2004).
15. P. W. Reddien, A. L. Bermange, K. J. Murfitt, J. R. Jennings, A. Sánchez Alvarado, *Dev. Cell* **8**, 635 (2005).
16. J. Baguñà, E. Saló, C. Auladell, *Development* **107**, 77 (1989).
17. G. T. Eisenhoffer, H. Kang, A. Sánchez Alvarado, *Cell Stem Cell* **3**, 327 (2008).
18. P. A. Newmark, A. Sánchez Alvarado, *Dev. Biol.* **220**, 142 (2000).
19. A. Salvetti *et al.*, *Dev. Biol.* **328**, 305 (2009).
20. C. S. Lange, C. W. Gilbert, *Int. J. Radiat. Biol.* **14**, 373 (1968).
21. E. Wolff, F. Dubois, *Rev. Suisse Zool.* **55**, 218 (1948).
22. Materials and methods are available as supporting material on *Science* Online.
23. A. J. Becker, E. A. McCulloch, J. E. Till, *Nature* **197**, 452 (1963).
24. J. E. Till, E. A. McCulloch, *Radiat. Res.* **14**, 213 (1961).
25. T. Guo, A. H. Peters, P. A. Newmark, *Dev. Cell* **11**, 159 (2006).
26. P. W. Reddien, N. J. Oviedo, J. R. Jennings, J. C. Jenkin, A. Sánchez Alvarado, *Science* **310**, 1327 (2005).
27. T. D. Hewitson, K. J. Kelynack, I. A. Darby, *Methods Mol. Biol.* **326**, 219 (2006).
28. R. Bravo, R. Frank, P. A. Blundell, H. Macdonald-Bravo, *Nature* **326**, 515 (1987).
29. S. Eriksson, A. Gräslund, S. Skog, L. Thelander, B. Tribukait, *J. Biol. Chem.* **259**, 11695 (1984).

30. D. Wenemoser, P. W. Reddien, *Dev. Biol.* **344**, 979 (2010).
31. J. Baguñà, *J. Exp. Zool.* **195**, 53 (1976).
32. M. L. Scimone, J. Meisel, P. W. Reddien, *Development* **137**, 1231 (2010).
33. B. J. Pearson, A. Sánchez Alvarado, *Development* **137**, 213 (2010).
34. K. Nishimura, Y. Kitamura, T. Taniguchi, K. Agata, *Neuroscience* **168**, 18 (2010).
35. E. E. Morrisey *et al.*, *Genes Dev.* **12**, 3579 (1998).
36. C. R. Bardeen, F. H. Baetjer, *J. Exp. Zool.* **1**, 191 (1904).
37. F. Dubois, *Bull. Biol. Fr. Belg.* **83**, 213 (1949).
38. T. Lender, A. Gabriel, *C. R. Acad. Sc. Paris* **260**, 4095 (1965).
39. T. Hayashi, M. Asami, S. Higuchi, N. Shibata, K. Agata, *Dev. Growth Differ.* **48**, 371 (2006).

Acknowledgments: We thank D. Kim for manuscript comments; S. Lapan for neuronal and intestinal markers; M. Srivastava for phylogenetics advice; D. Wenemoser for SMEDWI-1 antibody purification; J. Owen for Illumina data; M. Griffin for flow cytometry assistance; and P. Hsu, G. Bell, R. Young, and all members of the Reddien Lab for extensive comments and discussion. P.W.R. is an early career scientist of the Howard Hughes Medical Institute and an associate member of the Broad Institute of Harvard and MIT. We acknowledge support from the NIH (grant R01GM080639) and the Keck Foundation.

Supporting Online Material
www.sciencemag.org/cgi/content/full/332/6031/811/DC1
Materials and Methods
Figs. S1 to S19
Table S1
References

8 February 2011; accepted 11 April 2011
10.1126/science.1203983

Computational Design of Proteins Targeting the Conserved Stem Region of Influenza Hemagglutinin

Sarel J. Fleishman,[1*] Timothy A. Whitehead,[1*] Damian C. Ekiert,[2*] Cyrille Dreyfus,[2] Jacob E. Corn,[1†] Eva-Maria Strauch,[1] Ian A. Wilson,[2] David Baker[1,3‡]

We describe a general computational method for designing proteins that bind a surface patch of interest on a target macromolecule. Favorable interactions between disembodied amino acid residues and the target surface are identified and used to anchor de novo designed interfaces. The method was used to design proteins that bind a conserved surface patch on the stem of the influenza hemagglutinin (HA) from the 1918 H1N1 pandemic virus. After affinity maturation, two of the designed proteins, HB36 and HB80, bind H1 and H5 HAs with low nanomolar affinity. Further, HB80 inhibits the HA fusogenic conformational changes induced at low pH. The crystal structure of HB36 in complex with 1918/H1 HA revealed that the actual binding interface is nearly identical to that in the computational design model. Such designed binding proteins may be useful for both diagnostics and therapeutics.

Molecular recognition is central to biology, and high-affinity binding proteins, such as antibodies, are invaluable for both diagnostics and therapeutics (*1*). Current methods for producing antibodies and other proteins that bind a protein of interest involve screening large numbers of variants generated by the immune system or by library construction (*2*). The computer-based design of high-affinity binding proteins is a fundamental test of current understanding of the physical-chemical basis of molecular recognition and, if successful, would be a powerful complement to current library-based screening methods, because it would allow targeting of specific patches on a protein surface. Recent advances in computational design of protein interactions have yielded switches in interaction specificity (*3*), methods to generate modest-affinity complexes (*4*, *5*), two-sided design of a novel protein interface (*6*), and design of a high-affinity interaction by grafting known key residues onto an unrelated protein scaffold (*7*). However, the capability to target an arbitrarily selected protein surface has remained elusive.

Influenza presents a serious public health challenge, and new therapies are needed to combat viruses that are resistant to existing antiviral medicines (*8*) or that escape neutralization by the immune system. Hemagglutinin (HA) is a prime candidate for drug development as it is the major player in viral invasion of cells lining the respiratory tract. Although most antibodies bind to the rapidly varying head region of HA, recently two antibodies, CR6261 and F10, were structurally characterized (*9*, *10*) and found to bind to a region on the HA stem, which is conserved among all group 1 influenza strains (fig. S1) (*11*). Here, we describe a computational method for designing protein-protein interactions de novo and use the method to design high-affinity binders to the conserved stem region on influenza HA.

Computational Design Method

In devising the computational design strategy, we considered features common to dissociable protein complexes. During protein complex formation, proteins bury on average ~1600 Å^2 of solvent-exposed surface area (*12*). Interfaces typically contain several residues that make highly optimized van der Waals, hydrogen bonding, and electrostatic interactions with the partner protein; these interaction hot spots contribute a large fraction of the binding energy (*13*).

Our strategy thus centers on the design of interfaces that have both high shape complementarity and a core region of highly optimized, hot spot–like residue interactions (*14*). We engineered high-affinity interactions and high shape complementarity into scaffold proteins in two steps (see Fig. 1): (i) disembodied amino acid residues were computationally docked or positioned against the target surface to identify energetically favorable configurations with the target surface; and (ii) shape-complementary configurations of scaffold proteins were computed that anchor these energetically favorable interactions.

Design of HA-Binding Proteins

The surface on the stem of HA recognized by neutralizing antibodies consists of a hydrophobic groove that is flanked by two loops that place severe steric constraints on binding to the epitope (Fig. 2, A and B) (*15*). In the first step of our design protocol (Fig. 1), the disembodied hot spot residues found through computational docking cluster into three regions contacting HA (HS1, HS2, and HS3) (Fig. 1). In HS1, a Phe side chain forms an energetically favorable aromatic stacking interaction with Trp^{21} on chain 2 of the HA (HA2) (HA residue numbering corresponds to the H3 subtype sequence-numbering convention) (*16*). In HS2, the nonpolar residues Ile, Leu, Met, Phe, and Val, make favorable van der Waals interactions with both the hydrophobic groove and HS1 (Fig. 1 and fig. S2). In HS3, a Tyr side chain forms a hydrogen bond to Asp^{19} on HA2 and van der Waals interactions with the A helix on HA2. The Tyr in HS3 resembles the conformation of a Tyr residue observed on the antibody in the structure of the HA and CR6261 Fab complex (figs. S1 and S2); the HS1 and HS2 interactions are not found in the antibody structures (*9*, *10*, *17*) (fig. S1).

In the second step, we searched a set of 865 protein structures selected for ease of experimental manipulation (*18*) (table S1) for scaffolds capable of supporting the disembodied hot spot residues and that are shape complementary to the stem region. Each scaffold protein was docked against the stem region using the feature-matching algorithm PatchDock (*19*), which identified hun-

[1]Department of Biochemistry, University of Washington, Seattle, WA 98195, USA. [2]Department of Molecular Biology and the Skaggs Institute for Chemical Biology, The Scripps Research Institute, 10550 North Torrey Pines Road, La Jolla, CA 92037, USA. [3]Howard Hughes Medical Institute, University of Washington, Seattle, WA 98195, USA.

*These authors contributed equally to this manuscript.
†Present address: Genentech, 1 DNA Way, South San Francisco, CA 94080, USA.
‡To whom correspondence should be addressed. E-mail: dabaker@uw.edu